BOUNDARY ARTIFACT REDUCTION IN WAVELET IMAGE COMPRESSION

D. Černá, V. Finěk, M. Gottfried, P. Hübnerová, S. Paulusová, J. Róža, L. Viščur

Department of Mathematics and Didactics of Mathematics, Technical University in Liberec

Abstract

In our contribution, we compute new edge wavelet filters for image compression and we compare errors for several image compression techniques. Our numerical experiments confirm the theoretical assumption that the error of the compression is smaller for the discrete wavelet transform with derived edge filters than for other methods using an extension of an image.

1 Introduction

Compression is important both for speed of transmission and efficiency of the storage of an image. A wavelet-based image compression has several advantages over an image compression using discrete cosine transform. It avoids blocking artifacts, it enables to achieve smaller compressed size for given quality and it facilitates progressive transmission of images.

A typical lossy wavelet image compression system consists of: discrete wavelet transform of the input image, thresholding and quantization of wavelet coefficients and entropy encoding. Originally, the discrete wavelet transform was designed for an infinite input data. However, images are usually defined over a rectangle. Therefore, applying the discrete wavelet transform directly leads to the artifacts near the boundary. There are several methods to handle this problem. They insist in padding of the image and applying discrete wavelet transform to the extended image: zero-padding (zpd), symmetrization (sym), antisymmetric padding (asym), smooth padding of order 0 or 1 (sp0, sp1), periodic-padding (ppd), wavelet periodization (per). An alternative approach insists in using the discrete wavelet transform directly but using special filters near the boundary (edge).

In our contribution, we compute new edge wavelet filters for image compression and we compare errors for several image compression techniques. Our numerical experiments confirm the theoretical assumption that the error of the compression is smaller for the discrete wavelet transform with derived edge filters than for other methods using an extension of an image.

2 Discrete wavelet transform

Wavelet transforms use a pair of biorthogonal functions ψ, $\tilde{\psi} \in L_2(\mathbb{R})$ and their dilated and shifted versions to analyze data. Biorthogonality means that

$$\left\langle \psi\left(\cdot - k\right), \tilde{\psi}\left(\cdot - l\right) \right\rangle = \delta_{kl}, \quad k,\ l \in \mathbb{Z}, \tag{1}$$

where $\langle \cdot, \cdot \rangle$ denotes an inner product in $L_2(\mathbb{R})$. The function ψ is called a *primal wavelet* and $\tilde{\psi}$ is a *dual wavelet*. Wavelets are associated with *scaling functions* ϕ, $\tilde{\phi} \in L_2(\mathbb{R})$. Scaling functions usually serve to represent a smooth part of data and they are obtained as a solution of scaling equations

$$\phi(x) = \sum_k h_k \phi(2x - k), \quad \tilde{\phi}(x) = \sum_k \tilde{h}_k \tilde{\phi}(2x - k), \tag{2}$$

coefficients h_k and $\tilde{h}_k$ are called *primal* and *dual scaling coefficients* or *filters*, respectively.

One of these wavelets is used to decompose the signal and the second one to reconstruct it. The numbers M, N of scaling coefficients for the scaling function ϕ and its dual $\tilde{\phi}$ may differ.

We want to create a biorthogonal system and therefore we require that

$$\sum_k h_k \widetilde{h}_{k+2l} = \begin{cases} 2 & \text{if } l = 0 \\ 0 & \text{otherwise.} \end{cases} \tag{3}$$

Then wavelets can be determined by wavelet equations as follows

$$\psi(x) = \sum_{k=0}^{N-1} (-1)^k \widetilde{h}_{N-1-k} \phi(2x-k) \tag{4}$$

and

$$\widetilde{\psi}(x) = \sum_{k=0}^{M-1} (-1)^k h_{M-1-k} \widetilde{\phi}(2x-k). \tag{5}$$

If $f \in L_2(\mathbb{R})$, and if we denote scaling coefficients of function f by $y_{j,k}$, and wavelet coefficients of function f by $x_{j,k}$ then

$$x_{j,k} := \langle f, \psi_{j,k} \rangle = \int_{\mathbb{R}} f(x) \psi_{j,k}(x)\, dx, \tag{6}$$

$$y_{j,k} := \langle f, \phi_{j,k} \rangle = \int_{\mathbb{R}} f(x) \phi_{j,k}(x)\, dx, \tag{7}$$

where $\phi_{j,k} := 2^{j/2}\phi\left(2^j \cdot -k\right)$ and $\tilde{\phi}_{j,k} := 2^{j/2}\tilde{\phi}\left(2^j \cdot -k\right)$. Thus the decomposition algorithm is achieved as follows

$$x_{j,k} \;=\; \frac{1}{\sqrt{2}} \sum_l (-1)^l\, h_{1-l}\, y_{j+1,2k+l} \tag{8}$$

and

$$y_{j,k} \;=\; \frac{1}{\sqrt{2}} \sum_l h_l\, y_{j+1,2k+l}. \tag{9}$$

This decomposition algorithm forms the first half of the discrete wavelet transform.

The reconstruction algorithms for the discrete wavelet transform is defined in this way

$$y_{l+1,k} = \frac{1}{\sqrt{2}} \sum_m \widetilde{h}_{m-2k} y_{l,m} + (-1)^m \widetilde{h}_{1-m-2k} x_{l,m}. \tag{10}$$

The discrete wavelet transform is also computationally very efficient, requiring only $O(n)$ operations, where n is the number of processed data.

The above DWT algorithm can be easily extended to any dimension by tensor products of a scaling function ϕ and a wavelet ψ. For instance, the two-dimensional biorthogonal algorithm is based on separate variables leading to prioritizing of horizontal, vertical and diagonal directions.

We define scaling function by $\phi(x,y) = \phi(x)\phi(y)$ and three wavelets by

- vertical wavelets: $\psi^1(x,y) = \phi(x)\psi(y)$,
- horizontal wavelets: $\psi^2(x,y) = \psi(x)\phi(y)$,
- diagonal wavelets: $\psi^3(x,y) = \psi(x)\psi(y)$.

It leads to one scaling and three wavelet sub-images at each resolution level. Then the part of decomposition algorithms is performed hereby

$$y_{j,k,l} \;=\; \frac{1}{\sqrt{2}} \sum_m \sum_n h_m\, h_n\, y_{j+1,2k+m,2l+n}. \tag{11}$$

Other part of the discrete biorthogonal wavelet transform are accomplished in a similar way. As an example, Figure 1 displays a 512×512 RGB image, each pixel quantized on 8 bits, i.e. 256 possible intensity levels for red, green and blue colour. A decomposition of the image on two levels is shown also in Figure 1. The coefficients of the coarsest approximation appear as a simplified version of the picture in the upper left corner. The rest of the array contains the absolute values of wavelet coefficients. Note that many of them are black, it means that they are close to $(0, 0, 0)$, and that we have mostly sparse representation, except near the edges.

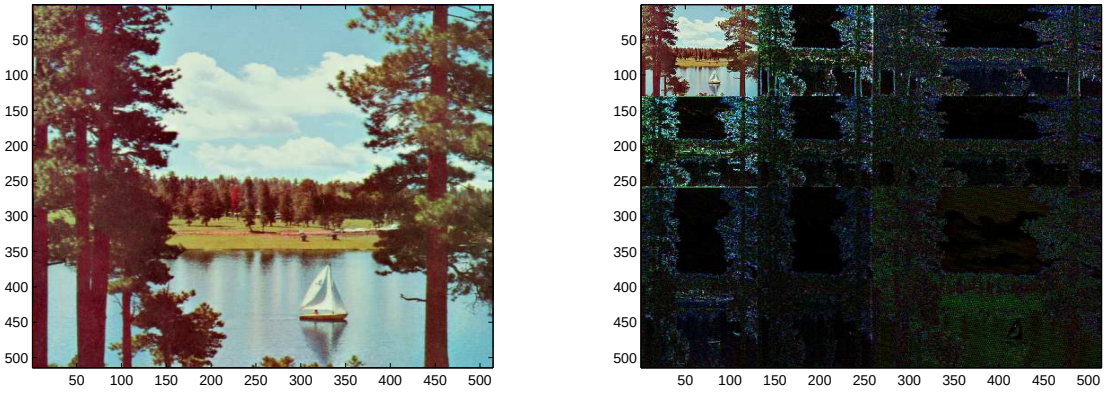

Figure 1: Image of a boat and its two-level decomposition.

3 Boundary artifact reduction

Until now, only wavelets over the real line have been mentioned, e.g. wavelets suitable to the analysis of signals defined over the whole line. However in most cases, we are working on compact intervals. Signals have finite support and images are usually defined over a rectangle. So we need to adapt wavelets from the real line to the compact interval. There are several methods to handle this problem. For instance:

- *Zero-padding (zpd):* This method assumes that the signal is zero outside the original support. The disadvantage of zero-padding is that discontinuities are artificially created at the boundary.
- *Symmetrization (sym):* This method assumes that signals or images can be recovered outside their original support by symmetric boundary value replication. Symmetrization has the disadvantage of artificially creating discontinuities of the first derivative at the border, but this method works well in general for images.
- *Antisymmetric padding (asym):* This method assumes that signals or images can be recovered outside their original support by antisymmetric boundary value replication.
- *Smooth padding of order 1 (sp1)* This method assumes that signals or images can be recovered outside their original support by a simple first-order derivative extrapolation: padding using a linear extension fit to the first two and last two values. Smooth padding works well in general for smooth functions.
- *Smooth padding of order 0 (sp0):* This method assumes that signals or images can be recovered outside their original support by a simple constant extrapolation. For a signal extension this is the repetition of the first value on the left and last value on the right.
- *Periodic-padding (ppd):* This method assumes that signals or images can be recovered outside their original support by periodic extension. The disadvantage of periodic padding is that discontinuities are artificially created at the border.

- *Wavelet periodization (per):* Wavelets supported completely inside the interval remain unchanged. Wavelets overlapping the boundary are divided into two pieces located at the left and right edges of the interval. This construction leads to large wavelet coefficients at the boundaries in the case that the periodized signal is not continuous.
- *Edge wavelets (edge):* Special edge wavelets are constructed to handle boundary effects explicitly. They are usually constructed by the method of stable completion [2] or by the lifting scheme [11]. However, it is a delicate task to design appropriate edge wavelets. None the less this approach is usually superior to others, because it does not assume the smoothness of the function nor the smoothness of its derivatives.

4 Edge biorthogonal filters

We derive edge filters corresponding to biorthogonal 3/5 filters from [5]:

$$\begin{aligned}
\mathbf{h} &= \frac{1}{4}(1,3,3,1), \\
\tilde{\mathbf{h}} &= \frac{1}{4}(-5,15,19,-97,-26,350,350,-26,-97,19,15,-5), \\
\mathbf{g} &= \frac{1}{4}(-5,-15,19,97,-26,-350,350,26,-97,-19,15,5), \\
\tilde{\mathbf{g}} &= \frac{1}{4}(-1,3,-3,1).
\end{aligned}$$

We use scaling functions and wavelets on the interval designed in [4]. The primal edge scaling filters $\mathbf{h}_1$ and $\mathbf{h}_2$ can be computed by solving the system:

$$\mathbf{P}_1 = \begin{pmatrix} \mathbf{h}_1 \\ \mathbf{h}_2 \end{pmatrix} \mathbf{P}_2, \tag{12}$$

where

$$\mathbf{P}_1 = \begin{pmatrix} \phi_{0,-2}(0) & \phi_{0,-2}(1) & \phi_{0,-2}(2) & \phi_{0,-2}(3) \\ \phi_{0,-1}(0) & \phi_{0,-1}(1) & \phi_{0,-2}(2) & \phi_{0,-1}(3) \end{pmatrix} \tag{13}$$

and

$$\mathbf{P}_2 = \begin{pmatrix} \phi_{1,-2}(0) & \phi_{1,-2}(1) & \phi_{1,-2}(2) & \phi_{1,-2}(3) \\ \phi_{1,-1}(0) & \phi_{1,-1}(1) & \phi_{1,-1}(2) & \phi_{1,-1}(3) \\ \vdots & & & \vdots \\ \phi_{1,2}(0) & \phi_{1,2}(1) & \phi_{1,2}(2) & \phi_{1,2}(3) \end{pmatrix}, \tag{14}$$

where $\phi_{j,k}$ are scaling functions from [4]. We obtain

$$\mathbf{M}_L^T = \begin{pmatrix} \mathbf{h}_1 \\ \mathbf{h}_2 \end{pmatrix} = \begin{pmatrix} 1 & 0.5 & 0 & 0 & 0 & 0 \\ 0 & 0.5 & 0.75 & 0.25 & 0 & 0 \end{pmatrix}. \tag{15}$$

Let Φ_j and $\tilde{\Phi}_j$ denote the interval primal and dual scaling basis at the scale j, respectively. There exist *refinement matrices* $\mathbf{M}_{j,0}$ and $\mathbf{M}_{j,1}$ such that

$$\Phi_j = \mathbf{M}_{j,0}^T \Phi_{j+1}, \quad \tilde{\Phi}_j = \mathbf{M}_{j,1}^T \tilde{\Phi}_{j+1}. \tag{16}$$

Due to the length of support of primal scaling functions, the refinement matrix $\mathbf{M}_{j,0}$ has the following structure:

$$\mathbf{M}_{j,0} = \frac{1}{\sqrt{2}} \begin{pmatrix} \mathbf{M}_L & & \\ & \mathbf{A}_j & \\ & & \mathbf{M}_R \end{pmatrix}, \tag{17}$$

where $\mathbf{A}_j$ is a $\left(2^{j+1}-2\right)\times\left(2^j-2\right)$ matrix given by

$$\begin{aligned}\left(\mathbf{A}_j\right)_{m,n} &= h_{m+1-2n}, \quad n=1,\ldots,2^j-2,\ 0\le m+1-2n\le 3,\\ &= 0, \qquad\qquad \text{otherwise.}\end{aligned} \tag{18}$$

To compute the refinement matrix corresponding to the dual scaling functions, we need to identify first the structure of refinement matrices $\mathbf{M}_{j,0}^{\Theta}$ corresponding to Θ.

$$\mathbf{M}_{j,0}^{\Theta}=\frac{1}{\sqrt{2}}\begin{pmatrix}\mathbf{M}_L^{\Theta} & & \\ & \tilde{\mathbf{A}}_j & \\ & & \mathbf{M}_R^{\Theta}\end{pmatrix}, \tag{19}$$

where $\mathbf{M}_L^{\Theta}$ and $\mathbf{M}_R^{\Theta}$ are blocks 16×6 and $\tilde{\mathbf{A}}_j$ is a matrix of the size $\left(2^{j+1}-10\right)\times\left(2^j-10\right)$ given by

$$\left(\tilde{\mathbf{A}}_j\right)_{m,n}=\tilde{h}_{m-2n}, \quad 0\le m-2n\le 11. \tag{20}$$

The receipt for the computation of the dual edge scaling filters is Lemma 3.1 from [6] and the definition dual scaling functions from [4]. The results are given in Table 1.

Our next goal is to determine the corresponding edge wavelet filters. We follow a general principle called *stable completion* which was proposed in [2].

Definition 1. Any $\mathbf{M}_{j,1}: l_2\left(J_j\right)\to l_2\left(I_{j+1}\right)$ is called a *stable completion* of $\mathbf{M}_{j,0}$, if

$$\left\|\mathbf{M}_j\right\|, \left\|\mathbf{M}_j^{-1}\right\| = O\left(1\right), \quad j\to\infty, \tag{21}$$

where $\mathbf{M}_j:=\left(\mathbf{M}_{j,0},\mathbf{M}_{j,1}\right)$.

The idea is to determine first an initial stable completion and then to project it to the desired complement space. This is summarized in the following theorem [2].

Theorem 2. *Let Φ_j and $\tilde{\Phi}_j$ be primal and dual scaling basis, respectively. Let $\mathbf{M}_{j,0}$ and $\tilde{\mathbf{M}}_{j,0}$ be refinement matrices corresponding to these bases. Suppose that $\check{\mathbf{M}}_{j,1}$ is some stable completion of $\mathbf{M}_{j,0}$ and $\check{\mathbf{G}}_j=\check{\mathbf{M}}_j^{-1}$. Then*

$$\mathbf{M}_{j,1}:=\left(\mathbf{I}-\mathbf{M}_{j,0}\tilde{\mathbf{M}}_{j,0}^T\right)\check{\mathbf{M}}_{j,1} \tag{22}$$

is also a stable completion and $\mathbf{G}_j=\mathbf{M}_j^{-1}$ has the form

$$\mathbf{G}_j=\begin{pmatrix}\tilde{\mathbf{M}}_{j,0}^T\\ \check{\mathbf{G}}_{j,1}\end{pmatrix}. \tag{23}$$

Moreover, the collections

$$\Psi_j:=\mathbf{M}_{j,1}^T\Phi_{j+1}, \quad \tilde{\Psi}_j:=\check{\mathbf{G}}_{j,1}^T\tilde{\Phi}_{j+1} \tag{24}$$

form biorthogonal systems

$$\left\langle\Psi_j,\tilde{\Psi}_j\right\rangle=\mathbf{I}, \quad \left\langle\Phi_j,\tilde{\Psi}_j\right\rangle=\left\langle\Psi_j,\tilde{\Phi}_j\right\rangle=\mathbf{0}. \tag{25}$$

$\tilde{\mathbf{h}}_1$	$\tilde{\mathbf{h}}_2$	$\tilde{\mathbf{h}}_3$
1.076681594556	−0.286738824456	0.092026650437
0.675063935593	0.573477648963	−0.184053300905
−0.355093741418	1.384958722225	−0.114782451680
−0.284846646838	0.355022784773	0.712453956922
0.326444989466	−0.686029696258	1.086876489964
0.230298713532	−0.391937987767	0.373645360512
−0.336268052254	0.632600808632	−0.762375368071
−0.008536973303	−0.035958766331	0.079313532709
0.129052427572	−0.187126019980	0.189053675945
−0.025278310555	0.036653550306	−0.042726257895
−0.019956560965	0.028937013399	−0.022828088348
0.006652186988	−0.009645671133	0.007609362783
$\tilde{\mathbf{h}}_4$	$\tilde{\mathbf{h}}_5$	$\tilde{\mathbf{h}}_6$
−0.029858563030	0.006382699501	−0.000583175059
0.059717126076	−0.012765399005	0.001166350119
0.020094926444	−0.003539406954	0.000392479032
−0.179719031518	0.036149018881	−0.003510137334
−0.032886047243	0.002296778426	−0.000642305610
0.617720309841	−0.111797984967	0.012064849802
1.310049183710	−0.214468356338	0.078067479536
−0.093568183916	0.976502245490	−0.269754682401
−0.367082460662	1.007183979711	−0.078985111774
0.071902750027	−0.079736069772	0.968151902990
0.056765328968	−0.274180234578	0.967856250235
−0.018921776323	0.054564933339	−0.072185098408
0	0.041432037960	−0.267927178809
0	−0.013810679320	0.052480581416
0	0	0.041432037960
0	0	−0.013810679320

Table 1: Dual edge scaling filters for biorthogonal 3/5 wavelets.

To find the initial stable completion we use some ideas from [6], [8]. By a suitable elimination of the matrix $\mathbf{A}_j$ we will successively reduce the upper and lower bands from $\mathbf{A}_j$. The elimination matrices are of the form

$$H_j^{(2i-1)} := \operatorname{diag}\left(\mathbf{I}_{i-1}, \mathbf{U}_{2i-1}, \ldots, \mathbf{U}_{2i-1}, \mathbf{I}_2\right), \tag{26}$$

$$H_j^{(2i)} := \operatorname{diag}\left(\mathbf{I}_{3-i}, \mathbf{L}_{2i}, \ldots, \mathbf{L}_{2i}, \mathbf{I}_{i-1}\right), \tag{27}$$

where

$$\mathbf{U}_{i+1} := \begin{pmatrix} 1 & -\frac{h^{(i)}_{\lceil i/2\rceil}}{h^{(i)}_{\lceil i/2\rceil+1}} \\ 0 & 1 \end{pmatrix}, \quad \mathbf{L}_{i+1} := \begin{pmatrix} 1 & 0 \\ -\frac{h^{(i)}_{3-\lfloor i/2\rfloor}}{h^{(i)}_{3-\lfloor i/2\rfloor-1}} & 1 \end{pmatrix}. \tag{28}$$

We define

$$\mathbf{A}_j^{(i)} := \mathbf{H}_j^{(i)} \mathbf{A}_j^{(i-1)}. \tag{29}$$

After 3 elimination steps we obtain the matrix $\mathbf{A}_j^{(3)}$ which looks as follows

$$\mathbf{A}_j^{(3)} = \mathbf{H}_j \mathbf{A}_j = \begin{pmatrix} 0 & 0 & & 0 \\ 0 & 0 & & \\ b & 0 & & \\ 0 & 0 & & \\ 0 & b & & \\ \vdots & 0 & \ddots & \\ & & & b \\ 0 & & & 0 \end{pmatrix}, \quad \text{where} \quad \mathbf{H}_j := \mathbf{H}_j^{(3)} \dots \mathbf{H}_j^{(1)}, \tag{30}$$

with $b = \frac{2}{3}$. We define

$$\mathbf{B}_j := \left(\mathbf{A}_j^{(3)}\right)^{-1} = \begin{pmatrix} 0 & 0 & b^{-1} & 0 & 0 & 0 & \dots & & 0 \\ 0 & 0 & 0 & 0 & b^{-1} & 0 & \dots & & 0 \\ & & & & & & \ddots & & \\ & & & & & & & b^{-1} & 0 \end{pmatrix} \tag{31}$$

and

$$\mathbf{F}_j := \begin{pmatrix} 0 & 0 & & \\ 1 & 0 & & \\ 0 & 0 & & \\ 0 & 1 & & \\ \vdots & 0 & \ddots & \\ & & & 1 \\ & & & 0 \\ & & & 0 \end{pmatrix} \tag{32}$$

Then, we have

$$\mathbf{B}_j \mathbf{F}_j = \mathbf{0}. \tag{33}$$

After these preparations we define extended versions of the matrices $\mathbf{H}_j$, $\mathbf{A}_j$, $\mathbf{A}_j^{(3)}$, and $\mathbf{B}_j$ by

$$\hat{\mathbf{H}}_j := \begin{pmatrix} \mathbf{I}_2 & & \\ & \mathbf{H}_j & \\ & & \mathbf{I}_2 \end{pmatrix}, \quad \hat{\mathbf{A}}_j^{(3)} := \begin{pmatrix} \mathbf{I}_2 & & \\ & \mathbf{A}_j^{(3)} & \\ & & \mathbf{I}_2 \end{pmatrix}, \tag{34}$$

$$\hat{\mathbf{A}}_j := \begin{pmatrix} \mathbf{I}_2 & & \\ & \mathbf{A}_j & \\ & & \mathbf{I}_2 \end{pmatrix}, \quad \hat{\mathbf{B}}_j^T := \begin{pmatrix} \mathbf{I}_2 & & \\ & \mathbf{B}_j^T & \\ & & \mathbf{I}_2 \end{pmatrix}. \tag{35}$$

Note that $\hat{\mathbf{H}}_j$, $\hat{\mathbf{A}}_j$, $\hat{\mathbf{A}}_j^{(3)}$, and $\hat{\mathbf{B}}_j$ are all matrices of the size $(\#\mathcal{I}_{j+1}) \times (\#\mathcal{I}_j)$. Hence, the completion of $\hat{\mathbf{A}}_j^{(3)}$ has to be a $(\#\mathcal{I}_{j+1}) \times 2^j$. We define an expanded version of $\mathbf{F}_j$ as follows:

$$\hat{\mathbf{F}}_j := \sqrt{2} \begin{pmatrix} & \mathbf{O} & \\ 1 & & \\ & \mathbf{F}_j & \\ & & 1 \\ & \mathbf{O} & \end{pmatrix} \begin{matrix} \} 2 \\ \\ \\ \\ \} 2 \end{matrix}. \tag{36}$$

The above findings can be summarized as follows.

$\mathbf{g}_1$	$\mathbf{g}_2$	$\mathbf{g}_3$
0.358006714919	0.285113393082	−0.239789603949
−0.418930417110	−0.146181763445	0.099525577556
0.203697087422	−0.218955991873	0.199033965888
0.002826360543	0.498085864326	−0.280579620459
−0.065289305020	−0.326958874104	−0.164217202965
−0.000649909267	−0.027423540495	0.548121218371
0.022059872669	0.085576352191	−0.302154238864
0.002840040788	0.012040803954	−0.048376908004
−0.004922768725	−0.017947844194	0.056788882014
−0.001228555869	−0.004389592253	0.013343131188
0.000463912919	0.001792150288	−0.006284808168
0.000154637640	0.000597383429	−0.002094936056

$\mathbf{g}_4$	$\mathbf{g}_5$
0.085295691728	−0.012543484077
−0.019191530639	0.002822283917
−0.061856449579	0.010053950918
0.061788157278	−0.006214251070
0.032053131410	−0.001841453148
−0.151061527183	0.023172344684
−0.008615979840	−0.018493973553
0.459389773437	−0.126840407858
−0.436869341495	0.031080662965
−0.030726657970	0.455269238917
0.122748096178	−0.455206521497
0.023554920948	−0.033679951610
−0.019531250000	0.126302083333
−0.006510416667	0.024739583333
0	−0.019531250000
0	−0.006510416667

Table 2: Primal edge wavelet filters for biorthogonal 3/5 wavelets.

Lemma 3. *The following relations hold:*

$$\hat{\mathbf{B}}_j \hat{\mathbf{A}}_j^{(3)} = \mathbf{I}_{\#\mathcal{I}_j}, \quad \frac{1}{2}\hat{\mathbf{F}}_j^T \hat{\mathbf{F}}_j = \mathbf{I}_{2^j} \tag{37}$$

and

$$\hat{\mathbf{B}}_j \hat{\mathbf{F}}_j = \mathbf{0}, \quad \hat{\mathbf{F}}_j^T \hat{\mathbf{A}}_j^{(N)} = \mathbf{0}. \tag{38}$$

The proof of this lemma is similar to the proof in [6]. Note that the refinement matrix $\mathbf{M}_{j,0}$ can be factorized as

$$\mathbf{M}_{j,0} = \mathbf{P}_j \hat{\mathbf{A}}_j = \mathbf{P}_j \hat{\mathbf{H}}_j^{-1} \hat{\mathbf{A}}_j^{(3)} \tag{39}$$

with

$$\mathbf{P}_j := \begin{pmatrix} \mathbf{M}_L & & \\ & \mathbf{I}_{\#\mathcal{I}_{j-5}} & \\ & & \mathbf{M}_R \end{pmatrix}. \tag{40}$$

Now we are able to define the initial stable completions of the refinement matrices $\mathbf{M}_{j,0}$.

Lemma 4. *Under the above assumptions, the matrices*

$$\check{\mathbf{M}}_{j,1} := \mathbf{P}_j \hat{\mathbf{H}}_j^{-1} \hat{\mathbf{F}}_j, \quad j \geq j_0, \tag{41}$$

are uniformly stable completions of the matrices $\mathbf{M}_{j,0}$. *Moreover, the inverse*

$$\check{\mathbf{G}}_j = \begin{pmatrix} \check{\mathbf{G}}_{j,0} \\ \check{\mathbf{G}}_{j,1} \end{pmatrix} \tag{42}$$

of $\check{\mathbf{M}}_j = \left(\mathbf{M}_{j,0}, \check{\mathbf{M}}_{j,1}\right)$ *is given by*

$$\check{\mathbf{G}}_{j,0} = \hat{\mathbf{B}}_j \hat{\mathbf{H}}_j \mathbf{P}_j^{-1}, \quad \check{\mathbf{G}}_{j,1} = \frac{1}{2} \hat{\mathbf{F}}_j^T \hat{\mathbf{H}}_j \mathbf{P}_j^{-1}. \tag{43}$$

The proof of this lemma is straightforward and similar to the proof in [6]. Then using the initial stable completion $\check{\mathbf{M}}_{j,1}$ we are already able to find wavelet filters according to the Theorem 2. Primal edge wavelet filters are listed in Table 2. There is only one edge dual wavelet filter $\left(\frac{2}{3}, -\frac{4}{3}, 1, -\frac{1}{3}\right)$.

5 Numerical examples

In this section, we compare errors for wavelet image compression techniques mentioned above. We compress an image of a boat, see Figure 1, and an image of peppers, see Figure 2.

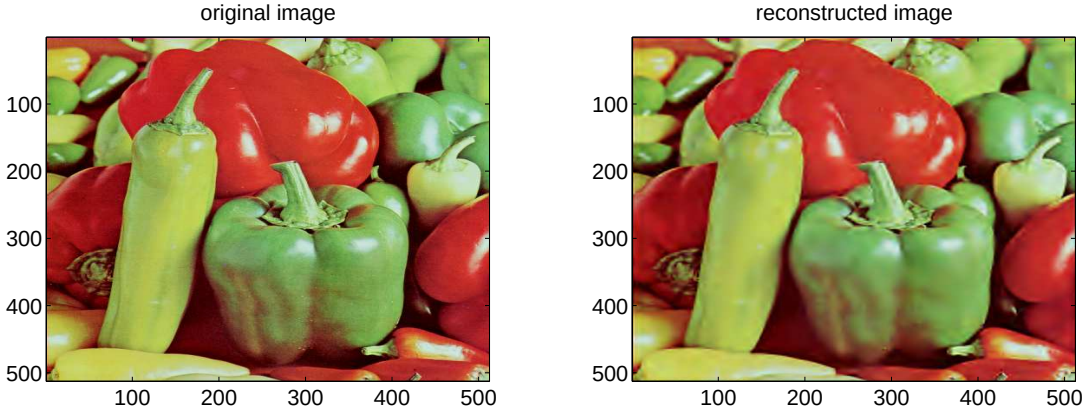

Figure 2: An original image of peppers and its reconstruction from 2% of wavelet coefficients.

We decompose the images on five levels using biorthogonal filters 3/5 from [5]. We compute the decompositions for several image extensions. We also apply discrete wavelet transform with special edge wavelet filters from the previous section. Then we threshold the wavelet coefficients greater than 100 and we reconstruct an image. Let I and $\hat{I}$ be arrays of the size $512 \times 512 \times 3$ characterizing colours in the original image and the reconstructed image, respectively. For several methods we compute

$$\mathrm{K} := \frac{\text{number of nonzero coefficients}}{\text{number of pixels in an original image}} \tag{44}$$

and

$$\text{relative error} := \sqrt{\frac{\sum_{k=1}^{3} \sum_{i,j=1}^{512} \left(I\left(i,j,k\right) - \hat{I}\left(i,j,k\right)\right)^2}{\sum_{k=1}^{3} \sum_{i,j=1}^{512} I\left(i,j,k\right)^2}}. \tag{45}$$

Furthermore, we compute the boundary error, i.e. the relative error for the area near the boundary. The results are given in Table 3. They confirm the theoretical assumption that the

error of the compression is smaller for the discrete wavelet transform with edge wavelets from [4] than for other methods using an extension of an image.

	Image of a boat				Image of peppers		
method	K	error	boundary error	method	K	error	boundary error
edge	0.0405	0.0873	0.0991	edge	0.0219	0.0672	0.0608
sym	0.0423	0.0895	0.1259	sym	0.0275	0.0705	0.0937
sp1	0.0442	0.0896	0.1289	sp1	0.0304	0.0706	0.0974
sp0	0.0340	0.0896	0.1297	sp0	0.0206	0.0708	0.0991
asym	0.0473	0.0909	0.1563	asym	0.0342	0.0727	0.1264
ppd	0.0474	0.0912	0.1607	ppd	0.0331	0.0740	0.1409
per	0.0290	0.0916	0.1637	zpd	0.0197	0.0740	0.1417
zpd	0.0314	0.0916	0.1698	per	0.0171	0.0736	0.1420

Table 3: Errors for several image compression methods.

Figure 3 shows the bottom right corner of the image of peppers and its reconstruction by several methods.

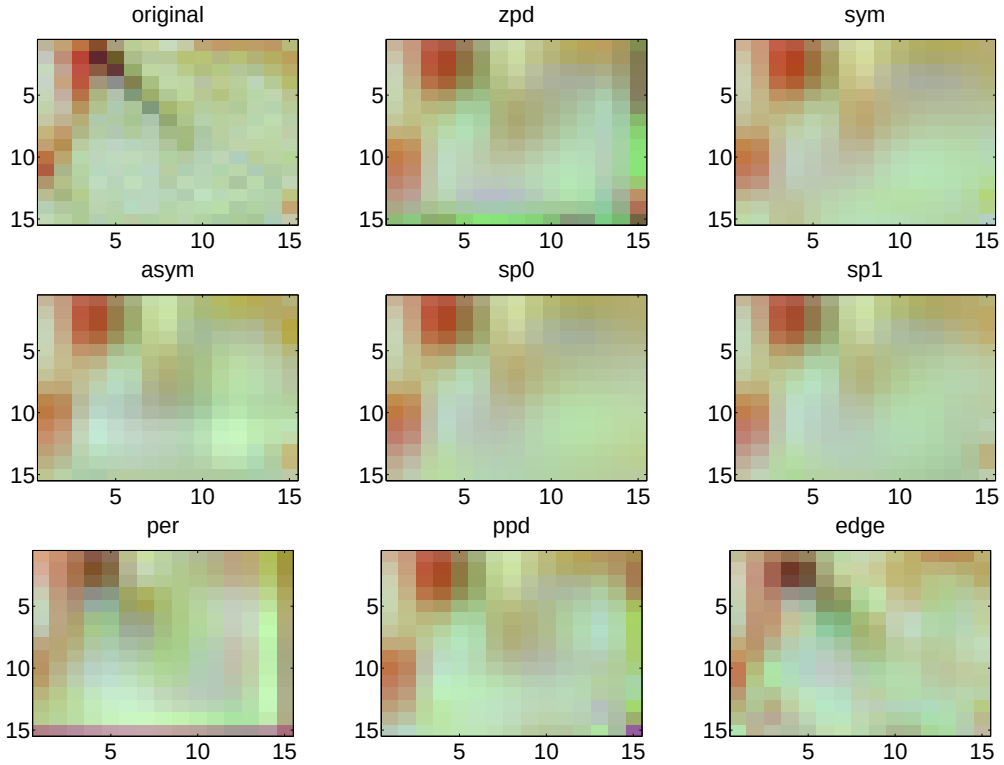

Figure 3: Part of an image of peppers and its reconstruction by several methods.

Acknowledgements. This work has been supported by the project IGS'09 financed by Technical University in Liberec. Authors gratefully acknowledge the support.

References

[1] Acharya, T.; Tsai, P. S.: *JPEG2000 standard for image compression: concepts, algorithms and VLSI architectures.* Wiley-Interscience, Hoboken, 2005.

[2] Carnicer, J.M.; Dahmen, W.; Peňa, J.M.: *Local decomposition of refinable spaces,* Appl. Comp. Harm. Anal. **6**, (1999), pp. 1-52.

[3] Černá, D.: *Stability of the boundary adapted wavelet transform.* In: ICPM'08, Liberec, 21-28, 2008.

[4] Černá, D.; Finěk, V.: *Optimized Construction of Biorthogonal Spline-Wavelets.* In: ICNAAM 2008 , AIP Conference Proceedings 1048, American Institute of Physics, New York: 134-137, 2008.

[5] Cohen, A.; Daubechies, I.; Feauveau, J.-C.: *Biorthogonal bases of compactly supported wavelets.* Comm. Pure and Appl. Math. 45: 485-560, 1992.

[6] Dahmen, W.; Kunoth, A.; Urban, K.: *Biorthogonal spline wavelets on the interval - stability and moment conditions.* Appl. Comp. Harm. Anal. 6: 132-196, 1999.

[7] Dahmen, W.; Kunoth, A.; Urban, K.: *Wavelets in numerical analysis and their quantitative properties.* In: A. Le Méhauté, C. Rabut, L. Schumaker (ed.): Surface fitting and multiresolution methods 2: 93-130, 1997.

[8] Dahmen, W.; Micchelli, C.A.: *Banded Matrices with Banded Inverses, II: Locally Finite Decomposition of Spline Spaces,* Constr. Appr. **9**, (1993), pp. 263-281.

[9] ISO/IEC 15444-1, *Information Technology-JPEG2000 Image Coding System, Part 1: Core Coding System*, 2000.

[10] ISO/IEC 15444-1, *Information Technology-JPEG2000 Image Coding System, Part 2: Extensions*, 2000.

[11] Sweldens, W.: *The Lifting Scheme: A Construction of Second Generation Wavelets*, SIAM J. Math. Anal. **29**, (1998), no. 2, pp. 511-546.

Dana Černá
Department of Mathematics and Didactics of Mathematics
Technical University in Liberec
Studentská 2
Liberec 461 17, Czech Republic
dana.cerna@tul.cz

Václav Finěk
Department of Mathematics and Didactics of Mathematics
Technical University in Liberec
Studentská 2
Liberec 461 17, Czech Republic
vaclav.finek@tul.cz